Available online at www.sciencedirect.com
ScienceDirect
Sensors and Actuators A 134 (2007) 427–435
SENSORS AND ACTUATORS A PHYSICAL
www.elsevier.com/locate/sna

PVDF corrugated transducer for ultrasonic ranging sensor

Minoru Toda [a,*], Jerry Dahl [b]

[a] *Measurement Specialties, Inc., 460 E. Swedesford Road, Ste. 2010, Wayne, PA 19087, USA*
[b] *General Dynamics, Corp., 4205 Westinghouse Commomn Drive, Charlotte, NC 28273, USA*

Received 30 November 2005; received in revised form 14 July 2006; accepted 17 July 2006
Available online 28 August 2006

Abstract

This paper describes a method to design and build ultrasonic transceivers using low-cost polyvinylidene fluoride (PVDF) corrugated film. The corrugated transducer features multiple curved sections, which provide a higher acoustic output compared to traditional ultrasonic transducer design using a single curved PVDF film section. We have built and demonstrated a prototype 200 kHz transducer and found it to be practical for applications requiring short-range distance measurement (20–300 mm) with SNR of 20 dB for 200 mm target. The prototype uses a single transducer that operated as both an ultrasonic transmitter and a receiver and provides a beam directivity of ±7° at −6 dB point using a 160 Vpp drive pulse. The transmitter output is 6.6 Pa (rms) at 30 cm with relative bandwidth of 33% and the receiver sensitivity is 0.55 mV/Pa. A microprocessor provides the timing signals, measures the time of flight from the transmitted pulse to the received echo, and calculates the distance.
© 2006 Elsevier B.V. All rights reserved.

Keywords: PVDF; Corrugated; Air ultrasonics; Distance measurement; Pulse echo

1. Introduction

Low-cost, short-range distance measurement sensors have a variety of commercial applications including toys, liquid-level and liquid-dispensing sensors, seat-occupancy detectors, human-body detectors for medical equipment, object-detection for automated mass production (robotics), etc. Most of commercially available air ultrasonic transducers are ceramic based and operate at 40 kHz. Transducers that operate at higher frequencies such as at 200 kHz are more limited and more expensive. However, various research reports in the range of 100 kHz to 5 MHz air ultrasonic transducer are available. Examples are for 1–3 connectivity ceramic composite [1], investigations of materials for matching layers [2], or electrostatic transducers [3].

Generally the overall sensitivity defined by receiver output versus unit voltage applied to transmitter is relatively low. At 30 cm separation and for 200 kHz commercial devices, the over all sensitivity is in the range of −60 to −70 dB. However, the resonance bandwidth is narrow (∼3%). In this work, PVDF ultrasonic transducers of small size (∼1 cm^2 area), high frequency (200 kHz), wide bandwidth (∼30%) and narrow beam (±7° at −6 dB) have been developed for a practical, low-cost, short-range measurement system for a target range of 20–300 mm. The overall sensitivity is lower (−90 to −86 dB) than ceramic transducers, but higher voltage pulses can be applied (up to 1000 Vpp) which provide 10–15 dB higher output than for ceramic transducers with maximum drive voltage. Therefore, using a high voltage transmitter drives significantly improves the receiver output and is comparable to that of ceramic transducers. In addition, the feature of wide bandwidth improves received signal even further if sharp pulses or coded signals are used.

Periodic concave–convex (corrugated) transducers using polyvinylidene fluoride (PVDF) were originally investigated and designed for large-area, high-intensity ultrasonic air transducers [4] that provided an ultra-highly-directional loudspeaker using a 40 kHz parametric array effect. Corrugated PVDF film transducers provide multiple sections of curved film, each having a common mechanical resonance. The structure is composed of single film with continuously formed multiple curved sections of a relatively large vibrating area. This corrugated design provides a higher acoustical output compared to a conventional circular film transducer. When the transducer is designed to operate in the 200–300 kHz range, it is difficult to accurately form the corrugation shape because of the fine periodicity. However, at lower frequencies the device size becomes too large because of the longer wavelength, and decreases the detection ability at

* Corresponding author. Tel.: +1 610 971 9893; fax: +1 610 971 9216.
E-mail address: minoru.toda@msiusa.com (M. Toda).

0924-4247/$ – see front matter © 2006 Elsevier B.V. All rights reserved.
doi:10.1016/j.sna.2006.07.018

short distances. For these reasons, 200–300 kHz is the optimal frequency range for short distance ranging sensor applications.

A number of researchers have investigated curved PVDF film transducers [5–11]. These transducers were designed using various structures including corrugated, curved film single section, cylindrical, multiple layers, disk, etc. In our design, the curved-film structure is equivalent to the half section of a cylindrical-film transmitter and the resonance frequency is inversely proportional to the film-curvature radius. This causes a relatively low output at higher frequencies because the small curvature radius leading to small transducer area.

Cylindrical film transmitters have also been investigated and reported to have a similar problem of a reduced output inversely proportional to the increasing frequencies [11]. In the case of ceramic transducers, multiple PZT plates embedded in polymer operated in length vibration mode (2–2 composite) were investigated for the 40–400 kHz range and designed for air-ranging application [12,13]. Another option is PZT disk transducers using radial-mode resonance (100–400 kHz) coupled with thickness-mode vibration. The output from radial-thickness coupled mode resonance is much stronger than from pure-thickness mode [14,15]. In this case a single transducer was used for both transmitter and receiver, and the drive/receive circuits were connected to the transducer through an electronic switch (TR switch).

Other researchers have built curved PVDF film-ranging sensors using separate transducers for the transmitter and receiver [5,8]. However, no one has succeeded in using a single PVDF transducer for both the transmitter and receiver. This paper reports the results of using a single corrugated transducer for both the transmitter and receiver.

It uses a novel TR diode switch to separate the transmitter and receiver functions and a 400 Vpp inductor–capacitor (PVDF) resonate drive circuit. Using a single transducer has the advantage of lower cost and size compared to using two transducers.

2. Basic design principle for corrugated transducers

Differential equations for curved piezoelectric film were solved and the detailed behaviors of vibrations and radiations were described in reference [7]. The same technique was applied to the corrugation transducer [4] with suitable boundary conditions; the resultant curves were obtained by numerical calculations. That process is mathematically rigorous but it cannot be reduced to simple useful relations. In this section, simple relations are derived from well-established concepts and useful equations are obtained, which help in the basic understanding and are also useful for design engineers.

2.1. Structure determination

A unique feature of PVDF is its length displacement along the molecular orientation direction (“1 direction”) induced by an electric field in the thickness direction. Because each section of PVDF film is curved in the 1 direction and has displacement in the length direction at the same time for all the section, the boundary line jointing each curved section cannot move at a high frequency and only allowed vibration direction is normal to the surface.

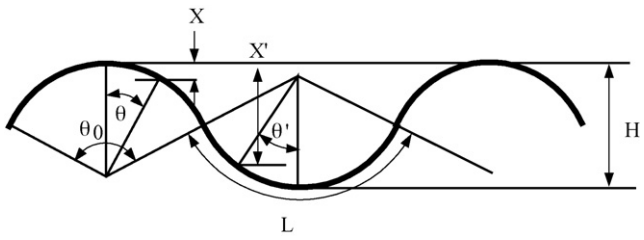

Fig. 1. A section of corrugation structure and parameters use for equations.

Because of the mass of the film and elasticity, curved PVDF film has mechanical resonance. In this model, the effect of higher order mode was neglected. As described in the basic theory [4,16] of single section of curved PVDF film, the fundamental resonance frequency f_0 is determined by the curvature radius R:

$$f_0 = \left(\frac{1}{2\pi R}\right)\sqrt{\frac{Y}{\rho_p}} \quad (1)$$

where Y is the Young’s modulus averaged over each layer and weighted for film thicknesses, and ρ_p is density averaged in the same way. For PVDF, $\sqrt{Y/\rho_p}$ is 1500 m/s and $R = 1.2$ mm for a 200 kHz transducer design. In practice, the silver ink used on the film influences both Y and ρ_p and better approximation values are $\sqrt{Y/\rho_p} = 1260$ m/s for 10 μm thick silver ink and $R = 1.0$ mm.

The basic concept for transducer design is the peak-to-valley corrugation height and is roughly equal to the half wavelength. The concave and convex regions vibrate with a 180° phase difference. However, the vibration is not only present at the top and bottom of the corrugation, but rather is spread over almost all the surface; the acoustic radiation is the sum of all the radiation from all the points. Therefore, the effective height, giving the 180° propagation path, should be less than actual height measured by peak to valley, and the exact height of corrugation should be a little more than a half wavelength (=0.86 mm) at 200 kHz. This optimum height both maximizes the output level and minimizes the side lobes as described in reference [4] in which case the frequency was ~40 kHz. The structure used in this experiment has a corrugation height of 1.0 mm and the half wavelength is 86% of the height. This was experimentally determined by making different corrugation height with same R to choose one structure with highest output and lowest sidelobes, in which case resonance frequency (half wavelength) was almost constant because R was constant.

The numerical calculations in reference [4] show that 69% of the optimum corrugation height is equal to the half wavelength (see Fig. 8, curve F at 54 kHz) where the corrugation wave shape is sinusoidal. In this work, the shape of corrugation are jointed circles, as in Fig. 1, which have flatter regions at the top and bottom areas, making the half wavelength 86% of the height.

2.2. Performance of the optimized corrugated PVDF transducer

2.2.1. Transmitter

The detailed theoretical results and the output from corrugated PVDF transducers were described in reference [4] for cases where the transducer area and periodicity were constant and only the radius was varied. Below we have derived an approximate equation to predict the output for a given curvature radius and total area for the structure in Fig. 1. The equations were derived assuming that the operation frequency is at resonance and the vibration is in radial vibration mode with a constant amplitude over one curved section. Flexural vibration modes are neglected.

The sinusoidal radial displacement ΔR by an applied sinusoidal voltage V is:

$$\Delta R = Rd_{31}\ \mathrm{V/h} \tag{2}$$

where R is radius, d_{31} the piezoelectric strain constant, V the applied sinusoidal voltage, and h is thickness of film [11].

This equation is derived from the basic piezoelectric relation of $\Delta L/L = d_{31}$ V/h for stress free conditions and $L = R\theta_0$, where L is arc length and θ_0 is full angle of the arc or shape factor (Fig. 1).

The optimum corrugation height for circularly curved film that provides the highest acoustical output can be approximately calculated as follows. Assume that all the points of the area radiate the acoustic wave in all directions. However, the rays going from each point to a sufficiently distant observation point are parallel and all of the parallel rays are superposed at the observation point. The distance from each point on the film to the observation point is different because of the corrugation shape. Because of the difference in the path length of each ray, each wave has a different phase which partially cancels at the observation point. The phase differences are proportional to $\exp(-\mathrm{j}kx)$, where $k = \omega/V_S$ (V_S is propagation velocity 344 m/s at the room temperature of 24 °C [17] and x is difference in distance. Assume x to be the distance from an arbitrary radiation point to the plane tangent to the top of the corrugation as shown by a dotted line in Fig. 1. The expression of x is

$$x = R(1 - \cos\theta) \tag{3}$$

for the left side (convex region), and

$$x' = R\left(\cos\theta' + 1 - 2\cos\frac{\theta_0}{2}\right) \tag{4}$$

for the right side (concave region), where θ and θ' are the angles made by each radiation point and central axis. The averaged radiation from all the points on the convex and concave regions is

$$I = \left(\frac{1}{2R\theta_0}\right)\left\{\int \exp(-\mathrm{j}kx)R\,\mathrm{d}\theta - \int \exp(-\mathrm{j}kx')R\,\mathrm{d}\theta'\right\} \tag{5}$$

In this case, each ray density leaving $R\,\mathrm{d}\theta$ has an absolute magnitude of unity with a phase difference of $\exp(-\mathrm{j}kx)$ or $\exp(-\mathrm{j}kx')$.

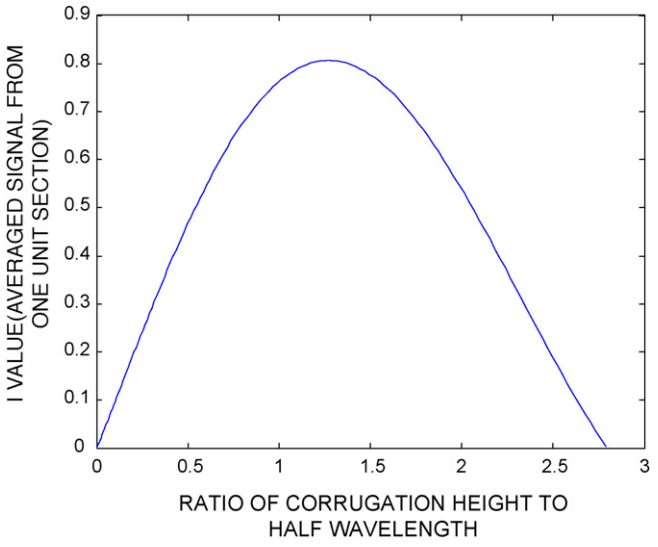

Fig. 2. Integrated value of I in (6) as a function of height H.

The total value for each ray was divided by $2R\theta_0$ to get the average. We can simplify Eq. (5) before integration by substituting $f = f_0$ (at resonance), $k = 2\pi f_0/V_S$ and using Eqs. (3) and (4) as below:

$$I = \left(\frac{1}{2\theta_0}\right)\left[\int \exp\left(\frac{-\mathrm{j}2\pi f_0 R(1-\cos\theta)}{V_S}\right)\mathrm{d}\theta - \int \exp\frac{-\mathrm{j}2\pi f_0 R(\cos\theta' + 1 - 2\cos\theta_0/2)}{V_S}\,\mathrm{d}\theta'\right] \tag{6}$$

From Eq. (1), f_0R is a constant, and the integration range of the first and second terms is from $-\theta_0/2$ to $\theta_0/2$. Thus, the form of Eq. (6) is only a function of θ_0 and the structural parameters (or resonance f_0) are not included.

Numerical integration of Eq. (6) was done for various values of θ_0, and it was found that the maximum value of magnitude of I is 0.809 at $\theta_0 = 0.6937\pi$. If phase differences did not exist, the I value should be unity; however, the reduction factor 0.809 is caused by the phase difference. In other words, the acoustic pressure from a corrugation transducer with the optimum shape is 80.9% of radiation from a piston vibrator with the same area.

At the optimal condition, the corrugation height H is given by

$$H = 2R\left(1 - \cos\frac{\theta_0}{2}\right) = 1.238\left(\frac{\lambda_0}{2}\right) \tag{7}$$

where λ_0 is the wavelength at f_0. Thus, the corrugation height should be 23.8% larger than half wavelength in this model. The I value of (6) versus $H/(\lambda_0/2)$ is plotted in Fig. 2 and it shows maximum at $H/(\lambda_0/2) = 1.24$.

Next, far-field acoustic pressure on the central axis normal to the transducer plane is calculated. If one ignores the phase term $\exp(-\mathrm{j}kx)$ or $\exp(-\mathrm{j}kx')$ of each ray, the acoustic pressure should be the total of radiation from all the vibrating points, which is roughly equal to that of piston radiator. This is because the acoustic pressure from the piston radiator is the sum of all the rays from all the vibrating points and all the rays on the point

on the central axis have almost the same phase if the point is sufficiently distant.

On the other hand, it is well known that the far-field acoustic pressure P radiated from an area A of a piston radiator at a distance D is given by:

$$P = \frac{f\rho_a A v}{D} \tag{8}$$

where ρ_a is the air density 1.29 kg/m^3 (see reference [13]) and v is the amplitude of the vibration velocity of the transducer. This equation can be applied to a corrugation transducer using $v = 2\pi f_0 \Delta R$ if we neglect the phase effect. Replacing f_0 and ΔR by use of Eqs. (1) and (2), the vibration velocity $v = \omega \Delta R$ can be expressed by

$$v = \left(\sqrt{\frac{Y}{\rho_p}}\right) d_{31}\ \text{V/h} \tag{9}$$

By substituting Eq. (9) into Eq. (8) and multiplying by the reduction ratio of 0.809, the acoustic pressure output of a corrugation transducer becomes:

$$P = 0.809 Q f_0 \rho_a A \left(\sqrt{\frac{Y}{\rho_p}}\right) d_{31}\ V/(hD) \tag{10}$$

As shown here, designing for a high-resonance frequency provides a higher output level for the same constant transducer area A.

In Eq. (10), Q is the quality factor, or the enhancement of the resonance effect and can be explained as follows. When the drive voltage is continuous or in bursts (more than 10 cycles), the vibration will grow at resonance. Therefore, at the resonance condition, ΔR becomes larger than that of Eq. (2). Let the enhancement factor at the resonance be Q. The Q value is a function of the mechanical loss of the layer material, acoustic loading due to radiation (radiation resistance), and the energy loss into the frame contacting at periphery of the film. These losses are difficult to measure separately, but it is possible to measure Q from the resonance bandwidth using $Q = f_0/\Delta f$, where Δf is the resonance width at the -3 dB points. A Q of $\sim$3 is observed in our experiments. For range sensors that use pulse drive, the transmit/receive signal does not grow fully and the enhancement of the resonance effect is less than the Q value.

The calculated transmitter output P with a 160 Vpp drive becomes 18.8 Pa-pp (6.6 Pa-rms) for: $Q = 3$, $F_0 = 200$ kHz, $\rho_a = 1.3$ kg/m^3, $A = \pi 0.0055^2 = 9.5 \times 10^{-5}$ m^2, $\sqrt{Y/\rho_p} = 1260$ m/s, $d_{31} = 14 \times 10^{-12}$ C/N, $h = 30$ μm, and $D = 0.3$ m.

2.2.2. Receiver

The sensitivity of corrugated film should be close to a curved clamped PVDF film element and was calculated by Naono et al. [16], where the reduction factor by the phase difference effect was neglected. The sensitivity equation is given below, which is Naono's equation modified by the reduction factor and the Q value:

$$V = 0.809 Q R P \left(\frac{d_{31}}{\varepsilon\varepsilon_0}\right) \tag{11}$$

where P is incoming acoustic pressure, ε the relative dielectric constant, and ε_0 is that of vacuum. In their calculations [16], they assumed that the acoustic pressure is constant over the film surface. In the case of corrugated film at the resonance condition, the phase difference on the film surface has to be taken into account and the same reduction factor has been used. Also, the resonance enhancement factor Q has to be multiplied. Since the directivity is much sharper than a single element device, the calculated sensitivity is valid only for normal incidence to the transducer plane.

The receiver sensitivity V/P is 5.48×10^{-4} V/Pa, for the parameters: $Q = 3$, $R = 1$ mm, $\varepsilon = 9$, and $\varepsilon_0 = 8.85 \times 10^{-12}$ F/m.

2.2.3. Transmitter and receiver combined sensitivity

For this case, the two corrugated transducers are separated by distance D and face each other. One of the transducer is set as the source and the acoustic wave transmitted across the air medium is received by the other transducer. The receiver output can be expressed by the product of Eqs. (10) and (11). The calculated receiver signal at 30 cm is 8.0 mVpp for the 160 Vpp drive.

Another method to calculate the acoustic pressure and the receiver output is described below. The reciprocity principle for a general circuit network having arbitrarily complicated branches is described as follows. Take any arbitrary two branches A and B. When a voltage source V is connected to branch A in series, it induces current I at branch B. Conversely, if the voltage source V is connected to branch B in series, it should induce the same current I to branch A. Herein, either A or B can be an acoustic port and the other port is an electric port. For an acoustic port, I and V correspond to velocity v and the pressure force $F_P = PA$ respectively.

At first the two terminals at the electrical input port are shorted and let it to be branch A, and V_A is connected to branch A in series. Branch B is an acoustic-output terminal at the face of the transducer with induced current I ($= v_B$). This v_B radiates an acoustic wave and causes an acoustic pressure P at the receiver face at distance D. The relationship between v_B and P is given by Eq. (8), using $v = v_B$.

Next, an incoming pressure force F_P (equivalent voltage source) is connected to branch B and branch A (with the shorted terminal) has current I'. From the reciprocity principle, relations of these quantities are:

$$\frac{v_B}{V} = \frac{I'}{F_P} \equiv \frac{V_{open}/Z_{in}}{PA} \tag{12}$$

where input impedance of branch A is Z_{in} and a relation $Z_{in}I' = V_{open}$ (open circuit voltage of branch A) has been used. Substituting (8) into (12), we get

$$v_B = \sqrt{\frac{VV_{open}/Z_{in}}{f\rho A^2/D}} \tag{13}$$

Using $Z_{in} = 1/j\omega C$ with $C = 400$ pF (impedance of PVDF is close to purely capacitive because of small electromechanical coupling constant), $V = 160$ Vpp, $V_{open} = 5$ mVpp (observed), we get $v_B = 0.227$ m/s at the transmitter's surface. When this radiates acoustic wave, the pressure at $D = 30$ cm is 18.7 Pa where Eq. (8) was used. From this, the received voltage at the open circuit condition is 8.0 mVpp where Eq. (11) was used. These results agree exactly with the earlier calculations of the receiver output with an acoustic pressure at $D = 30$ cm.

2.2.4. Directivity

A detailed theoretical calculation of the angular performance of a corrugated transducer was done in reference [1]. However, because of the similar device principle, it should be close to the directivity of a flat plate piston radiator, particularly for a near axial beam. This is because the acoustic waves from the top and bottom of the corrugation become in-phase during propagation and the axial acoustic wave should have the same appearance as a piston radiator. It is well known that the directivity of a circular flat piston is given by [17]:

$$F = \frac{2J_1(Z)}{Z} \quad \text{and} \quad Z = kr \sin\phi \tag{14}$$

where r is the radius of the piston radiator. Applying actual numbers of $r = 5.5$ mm and $f = 180$ kHz, the calculated 6 dB angle is: $\phi = \pm 7.0^\circ$.

3. Transducer structure and fabrication

The wave shape was formed by machining the sides of two circular ring holders. We conducted repeated experiments while varying the corrugation height and measuring the wave period to obtain the best performance, i.e., the highest output and the lowest sidelobes. The best structure was $H = 1$ mm at a frequency of 200 kHz ($\lambda = 1.7$ mm). These results were in close agreement with the calculated values. Once the equations were verified, we could determine the optimum wave shape for the ring holders. The two wavier surfaces were matched to hold the PVDF film in place to keep the corrugation shape. The two frames and the corrugated film were bonded with cyanoacrylate. We used PVDF film that was 30 μm thick and coated by 6 μm silver ink. Herein it should be noted that silver ink is featured by easy wire connection by use of riveted eyelets.

The effective area of the transducer had an 11 mm diameter and contained three periods of wave shape and is shown in Fig. 3.

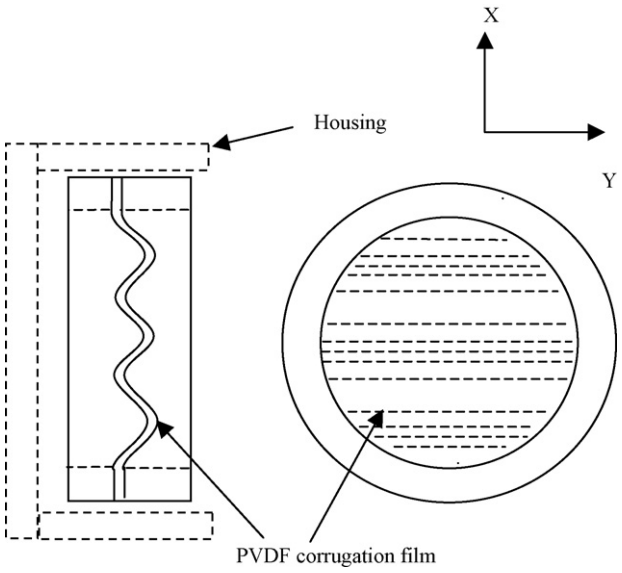

Fig. 3. Device structure. Diameter of effective area is 11 mm.

4. Measurement of the transducer performance

Normally the transmitter output is measured using a calibrated microphone. However, commercially available measurement microphones that extend to high frequency ranges are only calibrated up to about 130–160 kHz, depending on the model. Therefore, we could not use a commercial microphone to take accurate measurements at 200 kHz. Another problem arose in connection with measuring the receiver sensitivity. This could not be directly measured because receiver sensitivity is defined by the ratio of receiver output voltage to the incident acoustic pressure, which was outside the calibrated range of the microphone.

For these reasons, we measured the transducer sensitivity by combining two identical transducer pairs, one used as the transmitter and the other as the receiver, separated by 30 cm. A 15-cycle burst at 160 Vpp was applied to the transmitter and the receiver output was plotted as a function of the frequency, as shown in Fig. 4. In this measurement, the orientations of both transducers were adjusted for maximum output. We conducted experiments using two types of transducer mounting. One was the transducer without the external housing in which the wave from the back side was transmitted into the free space (plots by crosses). The other type allowed reflections from the back wall of the housing and a sharper resonance curve was formed (plots by "o" and "x").

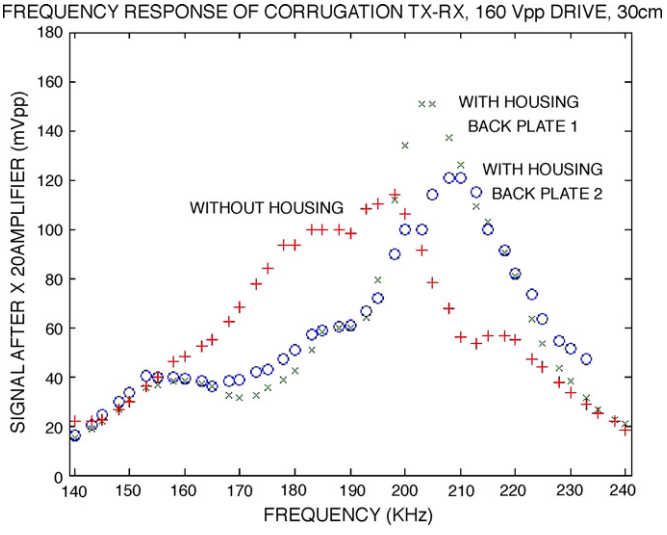

Fig. 4. Frequency response of transmitter and receiver (same device) separated 30 cm. Output is amplified by gain of 20. Circles and '×' are for transducers in housing and crosses are for one not in housing.

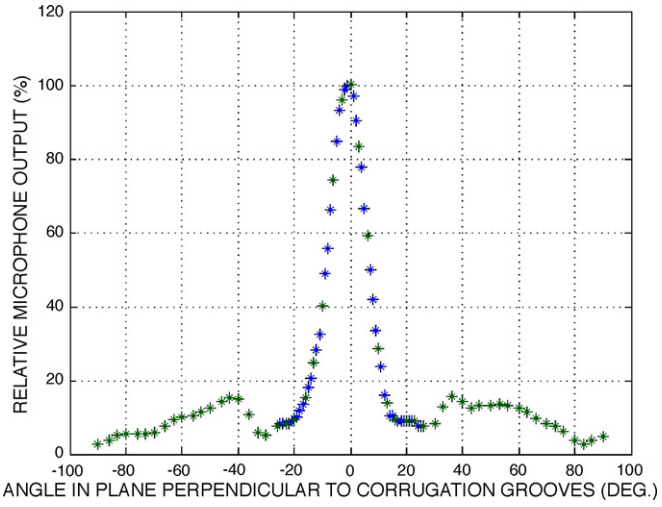

Fig. 5. Directivity is x–z plane (y axis is parallel to corrugation ridge).

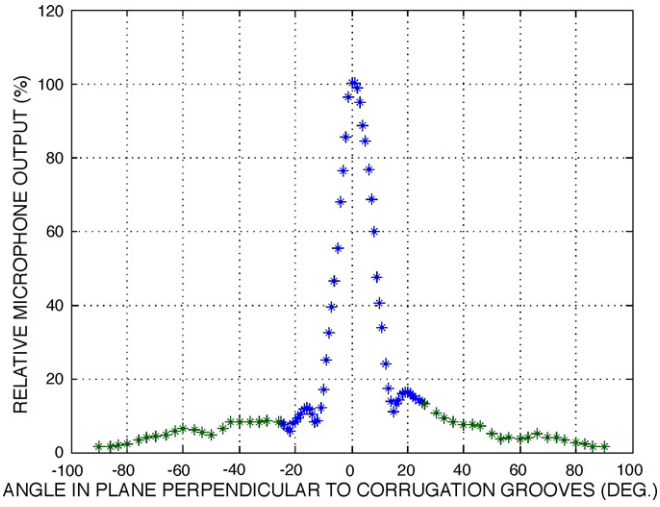

Fig. 6. Directivity in y–z plane(y axis is parallel to corrugation ridge).

For the reflected case, slight differences in the distance of the back-wall distance resulted in different output performance. The detailed back-wall effect was investigated but it generally adds added spurious peaks or valleys to the frequency response curves. When the transducer was operated in pulse mode for actual ranging sensor, the echo signal was not influenced by the back-wall position. This was because the spectrum of pulse is very broad, and the effects of peak and valley canceled each other. Therefore, we made no further efforts to design the housing to account for the effect of reflections.

At 200 kHz, the attenuation in air of 30 cm propagation is 3–4 dB, depending on the humidity. Therefore, if there was no attenuation, the observed peak signal of 5 mVpp would have become 7–8 mVpp, which agrees with the theoretical value. Generally, the Q value of a transducer is defined by the resonance frequency f_0 divided by resonance bandwidth $\Delta f'$ at -3 dB. In this case, however, the width at -6 dB was used because transmitter and receiver response curves were combined as a matched pair.

When the transmitter (without housing) was driven at 200 kHz and was rotated around the y axis, which is parallel to the ridge lines of the corrugation (Fig. 3), the variation of received signal from a microphone (model 4135, Bruel and Kjaer) was plotted as a function of the angle, as shown in Fig. 5. Note here that the microphone was not calibrated at the frequency and it was used for measurement of relative value when the signal varied. The main lobe becomes -6 dB at an angle of $\pm 7.6^\circ$ off from the averaged center. At -40 and $+35^\circ$ off from the center, there are small peaks of 16% and 17% of the main lobe. These are side lobes of typical corrugation transducer and to reduce further is difficult. If the corrugation height H is slightly off from the optimum condition, these peaks become ~30–50% of the main lobe. This means H at this condition is close to the optimum condition. In this measurement, the drive voltage was 400 Vpp in 15-cycle burst, separation between transducers was 30 cm, and transducers were not in housing.

When the transmitter was rotated around the x-axis, which is perpendicular to the ridge lines of corrugation (Fig. 3), and all other conditions were unchanged, the variation of received signal is shown in Fig. 6. In this case, peaks of the side lobe at 35–40° do not exist and the -6 dB point of the main lobe is at $\pm 7.0^\circ$.

A transducer was excited by a decaying sinusoidal signal with initial value of 800 Vpp, as shown in Fig. 7(a). The signal from the receiver at 30 cm is shown in Fig. 7(b), where gain of $\times 20$ was used and time scale is different from that of Fig. 7(a).

Design key parameters are summarized in Table 1, and observed values and theoretical values for a typical transducer pair are shown in Table 2.

Table 1
Design parameters used for comparison between theory and experimental observations

Design parameters	Values
Distance between transducers	30 cm
Drive waveform	160 Vpp 15 cycle burst
Transducer size	11 mm diameter
Size of housing	15 mm i.d. × 7.6 mm
Curvature radius of corrugation	1 mm

Table 2
Observed values and theoretical prediction for a pair of transducers

	Observed	Theoretical values
Actually received voltage	5 mVpp	
Received voltage corrected for propagation loss	7–9 mVpp	8 mVpp (without propagation loss)
Resonance frequency	190 kHz (210 kHz with housing)	200 kHz
Relative bandwidth at -6 dB	33% $Q=3$	
Directivity at -6 dB	± 7.0–7.6°	$\pm 7.0^\circ$

5. Application of PVDF corrugation transducer for practical ranging sensor

Ranging sensors use a transmitter that generates an acoustical pressure wave that propagates to the object. A portion of the

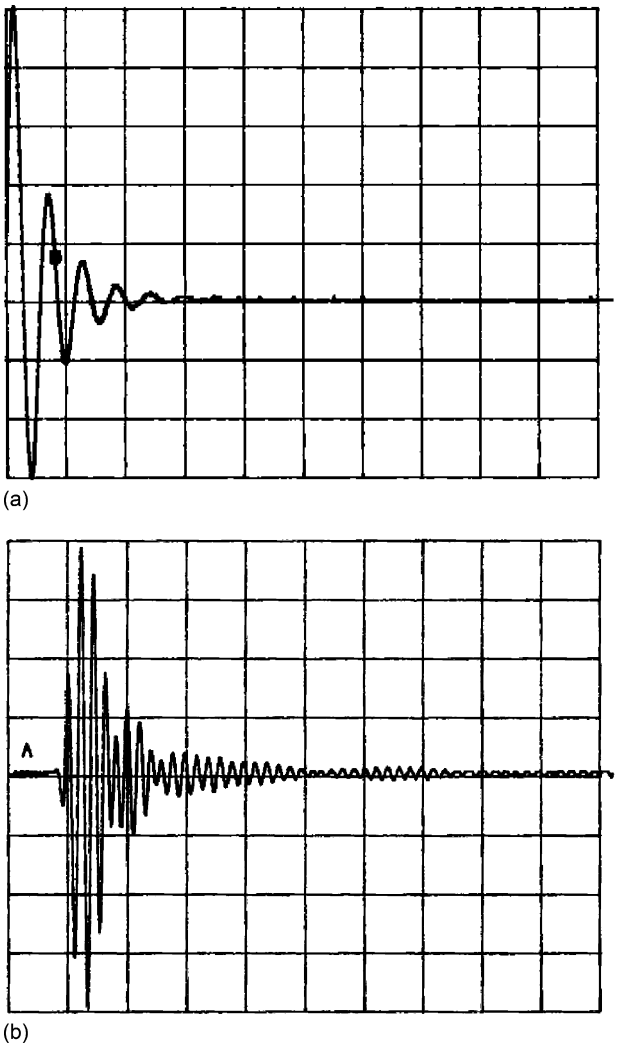

Fig. 7. (a) Drive waveform, 100 V/div and 10 μs/div (b) received waveform from a receiver at 30 cm, 20 mVpp/div with amplifier of gain 20 and 25 μs/div.

wave is reflected back to another transducer that operates as a receiver. The propagation time for the transmitted wave to reach and be reflected from the object and detected by the receiver is proportional to the distance traveled.

A practical sensor consists of a single transducer that is used for both the transmitter and receiver, a high-voltage driver, a receiver amplifier, an echo detector, and a microprocessor used for timing and control. The timing and control circuit starts the cycle by transmitting a high voltage pulse, waiting a short blanking period for the transducer to settle down, and measuring the time for the echo to be received. The microprocessor then calculates and outputs the distance based on the echo delay time.

5.1. Single transducer used as a transceiver

Ranging sensors often use separate transducers for the transmitter and receiver, particularly in the research setting. This is because the optimum transmitter and receiver structures are generally different and using separate devices often results in simpler electronics.

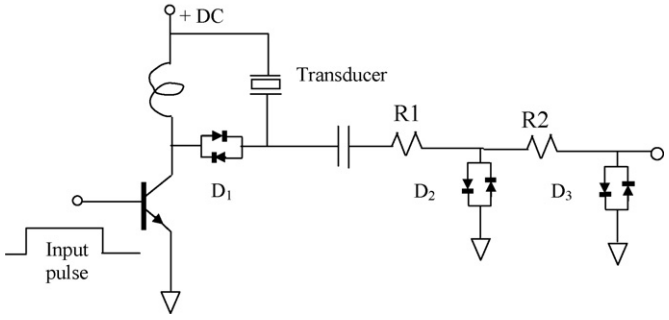

Fig. 8. Schematic circuit diagram for transient high voltage generator with diode transmit/receive mode switch.

However, for practical applications, the electronics cost are low compared to the transducer cost, and the economics are more important than optimum performance.

Therefore, a single transducer is often used for both transmitter and receiver. However, PVDF requires several hundred volts to drive the transducer in transmitting mode. If the high drive voltage (pulsed ac) couples to the receiver circuit, it could either damage or overload the amplifier; this concern precluded the use of a single transducer.

Saturation causes both a reduction in the amplifier gain and a delay for the amplifier to recover due to the charge-storage effect of the input transistors or the time constant of the coupling capacitor. Another problem of using a single transducer is that the received weak signal is attenuated by the low impedance of the drive power amplifier.

In order to use a single transducer as transmitter and receiver, a simple diode pair switching circuit is used to isolate the low impedance transmitter from the high impedance receiver circuit. The diodes are placed in series between the driver and the transducer, as shown in Fig. 8. The impedance of the diode pair D_1 becomes very low when the drive current flows into D_1 and it does not influence the V_P drive signal. During the driving period, the high V_P is attenuated from the receiver amplifier due to R_1, R_2 and diode pairs D_2 and D_3. During the blanking period, the drive current becomes zero, the impedance of D_1 becomes very high, and the drive transistor and inductor are isolated from the transducer. During this time, the impedance of D_2 and D_3 becomes very high and does not influence the received small signal.

5.2. High-voltage low-energy driver

The energy in a small inductor is used to generate a short high voltage decaying sinusoidal waveform to the transducer during the transmitting period. The drive signal quickly decays and the received signal is slightly lower than the calculated value obtained from the product of Eqs. (10) and (11) with $Q \sim 1$. The drive signal and the received signal are shown in Fig. 7(a and b).

In Fig. 9(a), when a current I_{dc} in the inductor is shut off, the stored energy in the inductor $E_L = LI_{dc}^2/2$ starts to flow out to the parallel capacitor. The charge energy at the peak voltage is $E_C = CV_C^2/2$. In Fig. 9(b), this charge flows back to the

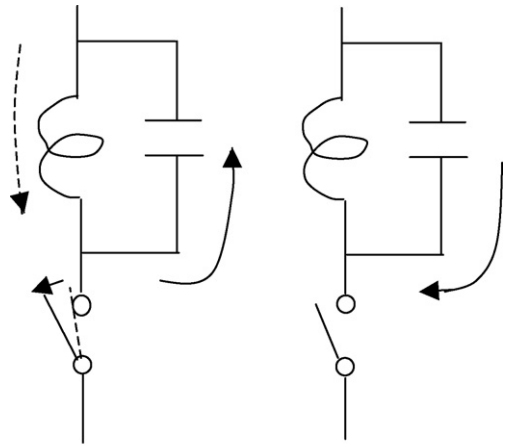

Fig. 9. (a) Right after dc current is shut off (b) half cycle later.

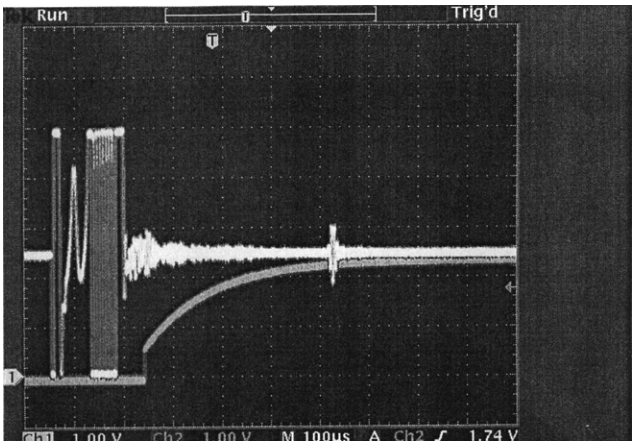

Fig. 10. Lower trace shows the threshold voltage changing with time, generated by charging a capacitor (1.0 V/div). Upper trace shows actual receiver output (1.0 V/div). The time scale is 100 μS/div and the reflection is from a target at 20 cm. The drive voltage was reduced by TR switch and echo signal was not.

inductor and again the current reaches its maximum. This current reverses direction and the voltage becomes zero when the current is maximized. This current again starts to flow into the capacitor and charges in the opposite polarity. The one-cycle frequency is determined by the inductor-capacitor parallel resonance, whose frequency is $\omega = 1/\sqrt{LC}$. The peak voltage decreases every cycle due to energy losses in the inductance (Ohmic loss in wire) and capacitance (dielectric loss). Therefore, the first cycle is the largest voltage and voltage decreases in the following cycles.

The initial peak voltage is determined by $E_L = E_C$ and is calculated by:

$$V_P = \sqrt{\frac{L}{C}} I_{dc} = \frac{I_{dc}}{\omega_0 C} \tag{15}$$

The initial peak voltage of V_P is determined by $I_{dc,}$ which is actually fed from a switching transistor. An initial peak value of V_P can be much larger than the dc source voltage, V_{dc}, if I_{dc} is large enough. After the switching transistor is turned on, the current starts to increase in time, following the well-known inductor transient current relationship,

$$I = \left(\frac{V_{dc}}{R}\right)\left[1 - \exp\left(\frac{-Rt}{L}\right)\right] \tag{16}$$

After the current increases to a certain value, and before the inductor saturates, the transistor is shut off. The instantaneous current before shutting off is I_{dc} and determines the magnitude of the high voltage.

5.3. Receiver amplifier

The amplifier is protected from the high voltage drive by clipping diodes D_2 and D_3. During the echo-receive time, the diodes are off and do not affect the signal. The amplifier is needed to increase the echo signal to a level that can be reliably detected.

To amplify the signal, a general purpose high frequency operational amplifier (LMH3344) was used. We selected a low-cost dual-op amp part with a bandwidth of 130 MHz. This allowed us to design a simple cascaded ac coupled amplifier, with each stage having a gain of 20.

5.4. Echo detection and dynamic threshold

We used the comparator inside the microprocessor to detect the amplified echo signal. One input to the comparator was connected to the amplifier and the other signal connected to the threshold voltage. When the echo-signal amplitude exceeded the threshold voltage, the comparator caused an interrupt signal to the microprocessor, signaling that an echo was detected.

After a pulse is transmitted, the drive signal and ringing noise quickly decays. In addition, the echo-signal amplitude decreases with distance and propagation time. When the target is close to the transducer, the time of flight is brief and reflection signal is fairly strong and appears in the region where the ringing voltage is decaying. For greater distances, the echo and ringing noise are lower. A dynamic threshold voltage allows the circuit to reliably detect the echo signals for both short and longer detection distances.

A resistor and capacitor network provided the dynamic time varying threshold voltage for the comparator. When the pulse is transmitted and during the blanking period, the capacitor is discharged by the microprocessor. During the echo sense period, the capacitor is exponentially charged by the pull-up resistor. This voltage at the charging capacitor voltage provides the time varying threshold voltage for the detection comparator, as shown by the lower trace which intersects the lower part of the echo signal (Fig. 10). This provides a larger noise margin for short distances when the echo and ringing noise are stronger and a smaller margin for longer distances when the echo and ringing noise are smaller. The upper trace in Fig. 10 shows the actual receiver output signal with SNR of 20 dB for a target at 20 cm. The initial large swing is drive voltage shunted by the diodes of the TR switch. The transducer's mechanical Q is ~3 and therefore the relative bandwidth of the amplifier should be more than ~50%. If the

bandwidth is narrower than this, the received signal becomes smaller.

5.5. Timing and control

A low-cost 8-bit Atmel ATiny 12 microprocessor was used for this circuit, but any general purpose microprocessor that contains a comparator can be used. An analog-to-digital comparator (ADC) is not needed.

The microprocessor software runs in a continuous loop that controls the pulse time, waits for a short blanking time, and starts a high speed timer. When the echo is detected, the timer is stopped and the distance is calculated from the timer value. The distance was outputted in a digital pulse width modulation (PWM) format where the pulse width indicated the distance.

6. Conclusion

Several PVDF corrugation transducers were designed for the 200 kHz operating region and the performance was measured for transmitter/receiver combination. Simplified design equations for corrugation transducers were proposed and the observed receiver output voltage agreed with the proposed equations and validate the equations for use in transducer design. The Eq. (10) for transmitter output predicts that the acoustic output pressure is proportional to the operation frequency when driven at resonance. The device was shown to be useful as a short-distance measurement sensor using a single transducer that performs both the transmit and receive function. A low-cost 8-bit microprocessor provided the timing and control signals.

References

[1] G. Heyword, A. Gauchagan, An evaluation of 1-3 connectivity composite transducers for air-coupled ultrasonic application, J Acoust. Soc. Am. 99 (4 Pt 1) (1996) 2148–2157.

[2] T.E. GometzAlvarez-Arenas, Acoustic impedance matching of piezoelectric transducers to air, IEEE Trans. Ultrason. Ferroelect. Freq. Contr. 51 (5) (2004) 624–633.

[3] D.A. Hutchins, D.W. Schindel, A.G. Bashford, W.D.M. Wright, Advance in ultrasonic electrostatic transduction, Ultrasonics 36 (1998) 1–6.

[4] M. Toda, Phase-matched air ultrasonic transducers using corrugated PVDF film with half wavelength depth, IEEE Trans. Ultrason. Ferroelect. Freq. Contr. 48 (6) (2001) 1568–1574.

[5] J.S. Schoenwald, J.F. Martin, PVF_2 transducers for acoustic ranging and imaging in air, in: 1983 IEEE Ultrasonic Symposium, 1983, pp. 577–580.

[6] F. Harnisch, N. Kroemer, W. Mathey, Ultrasonic transducers with piezoelectric polymer foil, Sens. Actuators A (25-27) (1991) 549–552.

[7] I. Veit, The piezoelectric PVDF film—its properties and application in electroacoustic transducers, in: 84th Convention Audio Engineering Society, Paris, France, 1988.

[8] A.S. Fiorillo, Design and characterization of a PVDF ultrasonic range sensor, IEEE Trans. Ultrason. Ferroelect. Freq. Contr. 39 (6) (1992) 688–692.

[9] R. Lerch, Electroacoustic transducers using piezoelectric polyvinylidene fluoride films, J. Acoust. Soc. Am. 66 (4) (1979) 952–954.

[10] M. Toda, S. Tosima, Theory of curved, clamped piezoelectricfilm, air-borne transducers, IEEE Trans. Ultrason. Ferroelect. Freq. Contr. 47 (6) (2000) 1421–1431.

[11] M. Toda, Cylindrical PVDF film transmitters and receivers for air ultrasound, IEEE Trans. Ultrason. Ferroelect. Freq. Contr. 49 (2002) 626–634.

[12] P. Kleinschmidt, V. Magori, Ultrasonic robotic-sensors for exact short range distance measurement and object identification, in: 1985 IEEE Ultrasonic Symposium, 1985, pp. 457–461.

[13] H. Emert, J. Schmolke, G. Weth, An adaptive ultrasonic sensor for object identification, in: 1986 IEEE Ultrasonic Symposium, 1986, pp. 555–558.

[14] V. Magori, H. Walker, Ultrasonic presence sensors with wide range and high local resolution, IEEE Trans. Ultrason. Ferroelect. Freq. Contr. 34 (2) (1987) 202–211.

[15] V. Magori, P.-C. Eccardt, H. Ruser, M. Vossiek, Directios-sensitive ultrasonic distance sensor using multimode stimulation of a single trasnsducer, in: 1995 IEEE Ultrasonic Symposium, 1995, pp. 1045–1049.

[16] H. Naono, T. Goto, M. Matsumoto, S. Ibaraki, Design of an electroacoustic transducer using piezoelectric polymer film, in: Audio Engineering Society Convention, New York, NY, November 4–7, 1977.

[17] J. Saneyoshi, Y. Kikuchi, O. Nomoto, Handbook of Ultrasonic Technology, Nikkan Kougyou News Paper Publishing, or www.sengpielaudio.com/calculator-speedsound.htm, 1980 (in Japanese).